



OPEN

Exploring the application value of ultrasound in animal studies of stem cell therapy for intrauterine adhesions

Siqi Guo¹, Wencong Li¹, Xiaoran Chen² & Meijuan Liu²✉

Endometrial damage leads to intrauterine adhesions (IUA), significantly impairing endometrial receptivity and fertility. Stem cell therapies, particularly umbilical cord mesenchymal stem cell (UC-MSCs), have shown promise in regenerating damaged endometrium, but prior studies have relied on ex vivo pathological evaluations. Ultrasound, as a non-invasive examination method, provides an important basis for the diagnosis, treatment and prognostic assessment of uterine adhesions in clinical practice. A series of statistical techniques were systematically used in this study, one-way ANOVA test, LSD-t test, Mann Whitney U test, Dunn's t test, and linear regression, with the aim of investigating whether ultrasound can effectively assess the effect of rat IUA model after treatment with IUA. This was an animal study involving 30 female Sprague-Dawley rats randomly divided into three groups: normal ($n=10$), IUA model ($n=10$), and UC-MSC therapy ($n=10$). The study duration was approximately three months, including UC-MSC administration and post-treatment follow-up. IUA was induced in the model and UC-MSC groups by mechanical scraping of the uterine endometrium. Rats in the UC-MSC group received intrauterine infusions of UC-MSCs. Endometrial thickness, morphology, and continuity were evaluated pre- and post-treatment using ultrasound. Histological analysis, including H&E, Masson's staining, and CK immunohistochemistry, was performed after euthanasia. Endometrial thickness significantly increased in the UC-MSC group compared to the model group (0.34 ± 0.06 mm vs. 0.11 ± 0.03 mm, $p < 0.05$), while fibrosis was significantly reduced (15.11% vs. 28.14%, $p < 0.05$). The UC-MSC group exhibited improved endometrial morphology and glandular density compared to the model group ($p < 0.05$). Particularly Ultrasound findings of endometrial thickness, are significantly associated with pathological assessments ($r > 0.99$, $p < 0.0001$). This study demonstrates that ultrasound is a reliable, non-invasive tool for monitoring the therapeutic effects of UC-MSCs on endometrial regeneration *in vivo*.

Keywords Ultrasonography, Stem cell transplantation, Cell- and Tissue-Based therapy, Endometrium, Fibrosis

Abbreviations

IUA	Intrauterine adhesion
UC-MSCs	Umbilical cord mesenchymal stem cell
H&E	Hematoxylin & eosin
CK	Cytokeratin
ARRIVE	Animal Research: Reporting of In Vivo Experiments
GS	Gestational sac
SK	Skull
SP	Spine
AD	Abdomen
UC	Umbilical cord
EV	Endometrial volume
VI	Vascularization index

¹Department of School of Medical Imaging, Binzhou Medical University, Shandong, Yantai, China. ²Department of Ultrasound, Affiliated Yantai Yuhuangding Hospital of Qingdao University, Shandong, Yantai, Yantai, China. ✉email: yhdyylmj@163.com

FI	Blood flow index
VFI	Vascularization-blood flow index

The endometrium is a tissue with a high capacity for self-repair, undergoing periodic growth, shedding, and regeneration in response to fluctuations in estrogen and progesterone levels. However, damaged endometrium can lose its self-repair capability, leading to the occurrence of intrauterine adhesions (IUA). IUA, also known as adhesion syndrome, is pathologically characterized by partial or complete adhesion of the uterine cavity due to endometrial fibrosis¹. A thin endometrium (less than 7 mm) is considered a key factor in embryo implantation failure and is a major cause of secondary infertility in women²⁻⁷. Endometrial regeneration are essential for supporting embryo implantation.

In recent years, stem cell therapy has demonstrated positive effects in the treatment of various tissue and organ injuries. A substantial amount of animal experiment literature has confirmed the efficacy of stem cell therapy in the regeneration of endometrium⁸⁻¹⁴. Umbilical cord mesenchymal stem cells (UC-MSCs), derived from discarded neonatal umbilical cord tissue, are easy to be cultured in vitro and have been widely applied in stem cell transplantation studies.

Previous literature assessing endometrial repairment has all been conducted in vitro, where uterine cavity tissue was collected from dissected rats for clinical pathology and related research, making it impossible to effectively evaluate endometrial receptivity preoperatively. This article will explore for the first time whether ultrasound examination can be used to assess the endometrial receptivity in vivo in animal studies involving UC-MSCs for the treatment of IUA.

Materials and methods

Clinical tissue samples

All tissue samples in this experiment were obtained from the delivery room at Yantai Yuhuangding Hospital. Approximately 15 cm of umbilical cord from healthy full-term newborns delivered vaginally was collected. Before delivery, tests for infectious diseases such as hepatitis B, syphilis, mycoplasma, and chlamydia were conducted, all of which returned negative results. Consent was obtained from the mothers and their families prior to the collection of the umbilical cord samples, with informed consent forms duly signed. The collection process was conducted under sterile conditions, and the samples were immersed in umbilical cord stem cell culture medium. They were then transported in sterile 50 ml centrifuge tubes to the Central Laboratory of Yantai Yuhuangding Hospital at 4 °C, with separation completed within four hours. The use of these specimens was approved by the Ethics Committee of Yantai Yuhuangding Hospital (NO.2024-554).

Isolation and culture of UC-MSCs

UC-MSCs were obtained using the tissue block culture method¹⁵. In brief, a 14# medical forceps and a 10# medical ophthalmic forceps were used to carefully separate the umbilical cord from the umbilical blood vessels and the cord epithelium. The remaining tissue was cut into fragments of 1–2 mm¹⁶. The tissue pieces were laid flat in a 10 cm culture dish and placed in a 37 °C CO₂ incubator for 30 min. Afterward, 10 ml of complete culture medium for human umbilical cord mesenchymal stem cells was carefully added to the dish, which was then returned to the incubator for culture. Primary mesenchymal stem cells could be observed migrating out after approximately 7 days, and when they occupied 80–90% of the culture dish, cell passage or cryopreservation could be performed.

Flow cytometry identification of surface markers of umbilical cord mesenchymal stem cells

Third-generation UC-MSCs with good growth were selected and cultured to 90–99% confluence. Cells were centrifuged at 1000 rpm for 5 min, and the supernatant was discarded, adjusting the cell concentration to 5×10^6 mL. Seven EP tubes were numbered, with antibodies CD90-FITC, CD44-PE, CD105-PerCP-Cy5.5, and CD73-APC added to tubes 1 to 4, respectively. Tube 5 served as a blank control. Tube 6 contained a mixture of positive antibody isotype controls (mIgG1-FITC, mIgG1-PerCP-Cy5.5, mIgG1-APC) and negative antibody isotype controls (mIgG1-PE, mIgG2a-PE). Tube 7 was filled with a mixture of positive antibodies (CD90-FITC, CD105-PerCP-Cy5.5, CD73-APC) and negative antibodies (CD34-PE, CD11b-PE, CD19-PE, CD45-PE, HLA-DR-PE). The flow cytometer was operated, and Flow Jo software was used to analyze the cell phenotype.

Cell induction and differentiation assessment

UC-MSCs in the logarithmic growth phase were collected and seeded into 6 cm diameter culture dishes at cell densities of 2.0×10^4 cells/cm², 2.0×10^4 cells/cm², and 2.0×10^5 cells/cm². The cultures were maintained in a 37 °C, 5% CO₂ environment until they reached 80–90% confluence. The original culture medium was discarded, and differentiation induction media for adipogenic, osteogenic, and chondrogenic lineages were added. The medium was changed every 2–3 days, and after 21 days, the induction status was observed under a microscope. Oil Red O staining solution, Alizarin Red staining solution, and Alcian Blue staining solution were added to the adipogenic, osteogenic, and chondrogenic induction media, respectively, for staining. Images were captured under a microscope for induction assessment.

Experimental animals

Female Sprague-Dawley (SD) rats of SPF grade (provided by Jinan Pengyue Laboratory Animal Breeding Co., Ltd., License No.: SCXK (Lu) 20190003), aged 7 to 9 weeks of gestation, weighing 150–200 g, were kept in separate cages. The rats were housed under controlled conditions, including room temperature (23–25 °C), humidity of 40–60%, a light/dark cycle of 14 h/10 hours, with ad libitum access to food and water. They underwent 1–2 weeks of acclimatization, during which vaginal cytology was checked twice daily to monitor estrous cycle frequency

and regularity. A total of 30 rats with consistent estrous cycles were selected for the study. All animal experiments were conducted in strict accordance with the NIH Guide for the Care and Use of Laboratory Animals. The work has been reported in line with the ARRIVE guidelines 2.0. UC-MSCs and all animals studies have been approved by Ethics Committee of Yantai Yuhuangding Hospital (NO.2024–554). All methods were carried out in accordance with ARRIVE guidelines 2.0 and American Veterinary Medical Association (AVMA) Guidelines for the Euthanasia of Animals (2020). All procedures followed were in accordance with institutional guidelines and the research protocol approved by the institutional review board.

The experimental rats were randomly divided into three groups: the normal group ($n=10$), the model group (modeled by mechanical injury, $n=10$), and the UC-MSCs group (administered UC-MSCs at a dose of $2 \times 10^7/200\mu\text{L}$, $n=10$, suspended in 1 mL of sterile PBS were injected into the uterine cavity.) Random numbers were generated using the standard=RAND () function in Microsoft Excel. One week after the establishment of the intrauterine adhesion model, UC-MSCs were injected into the uterine cavity through intrauterine infusion. The minimise potential confounders such as the order of measurements and treatments. Four to five estrous cycles post-treatment, rats were killed by isoflurane asphyxiation, uterine samples were collected under anesthesia to assess endometrial conditions. Hematoxylin and Eosin (H&E) staining, Masson's staining, and CK immunohistochemical staining were performed to observe changes in endometrial thickness and morphology.

Establishment of the intrauterine adhesion (IUA) model

Vaginal exfoliated cells from the rats were collected daily at 7–8 AM and 3–4 PM for cycle monitoring. Female SD rats in estrus were anesthetized by inhalation with isoflurane. An incision approximately 2 cm long and 2 cm above the pubic symphysis was made, and the MR-s240-2 ophthalmic curette was used to perform comprehensive scraping of the uterine cavity. Scraping was stopped when significant congestion was observed in the uterine body and the uterine wall appeared rough, followed by a saline wash of the uterine cavity. During the first three days post-surgery, penicillin was administered via intramuscular injection at a dose of 200,000 IU per day. Tissue collection was strictly confined to the estrus phase to standardize hormonal status. Tissue samples were collected during the estrus phase of the third estrous cycle post-surgery for H&E staining, Masson staining, and CK immunohistochemical staining.

Measurement of histological indicators (Using imageJ image processing Software)

(1) Measurement of Endometrial Thickness: Photographs of each H&E stained section were taken under low power magnification using an optical microscope. Four points at right angles were selected in each section to measure the endometrial thickness, and the average value was calculated as the endometrial thickness.

(2) Counting Gland Number: The number of glands in each H&E stained section was counted and recorded as the number of endometrial glands in the rat's uterus.

(3) Calculating Endometrial Fibrosis Area Ratio: For each Masson stained section, four random high-power fields were selected, and the ratio of the fibrotic area in the endometrial stroma to the total area of the endometrial stroma and glands was calculated. The average of these ratios was recorded as the endometrial fibrosis area ratio.

(4) Measuring Average Optical Density of Endometrial CK Staining: Photographs of each CK stained section were taken under low power magnification using an optical microscope. The cumulative optical density value and total protein amount of each section were calculated to obtain the average optical density value.

Ultrasound measurement indicators

All rats in the normal, model, and UC-MSCs groups underwent measurement of endometrial thickness using a small animal ultrasound machine (Vinho VINNO6LAB, Suzhou, China) before dissection for each group. The endometrial morphology and continuity of the uterine cavity were also observed during this assessment.

Evaluation metrics

Prior to dissection, all rats in the normal, model, and UC-MSCs groups had their endometrial thickness measured using a small animal ultrasound machine (Vinho VINNO6LAB, 18 MHz, Suzhou, China) to observe endometrial morphology and continuity. After dissection, uterine tissues were collected for phenotypic analysis. H&E staining was used to assess the number of endometrial glands, Masson's staining was employed to evaluate the degree of endometrial fibrosis, and CK immunohistochemical staining was conducted to indicate keratin expression levels.

Statistical analysis

Normality test was conducted on the measurement data, and one-way ANOVA was used for analysis. Pairwise comparisons were performed using the LSD-t test. For data not conforming to a normal distribution, results were expressed as M (Q1 and Q3), and the Mann-Whitney U test was used for analysis, with Dunn's test applied for pairwise comparisons. A significance level of $P<0.05$ was considered statistically significant. Correlation and difference analyses were conducted using linear regression analysis.

Results

In vitro culture and phenotypic identification of UC-MSCs

Flow cytometry analysis of third-generation UC-MSCs revealed that over 95% of UC-MSCs were positive for the surface antigens CD73, CD44, and CD105, while CD34, CD45, CD31, and HLA-DR were negative (Fig. 1). UC-MSCs induced to differentiate into adipocytes formed lipid droplets that stained red with Oil Red O; osteogenic differentiation resulted in calcium nodules in the bone tissue that appeared orange after staining with Alizarin Red; and the glycosaminoglycans in the chondrogenic differentiated cartilage tissue stained blue with Alcian Blue (Fig. 2).

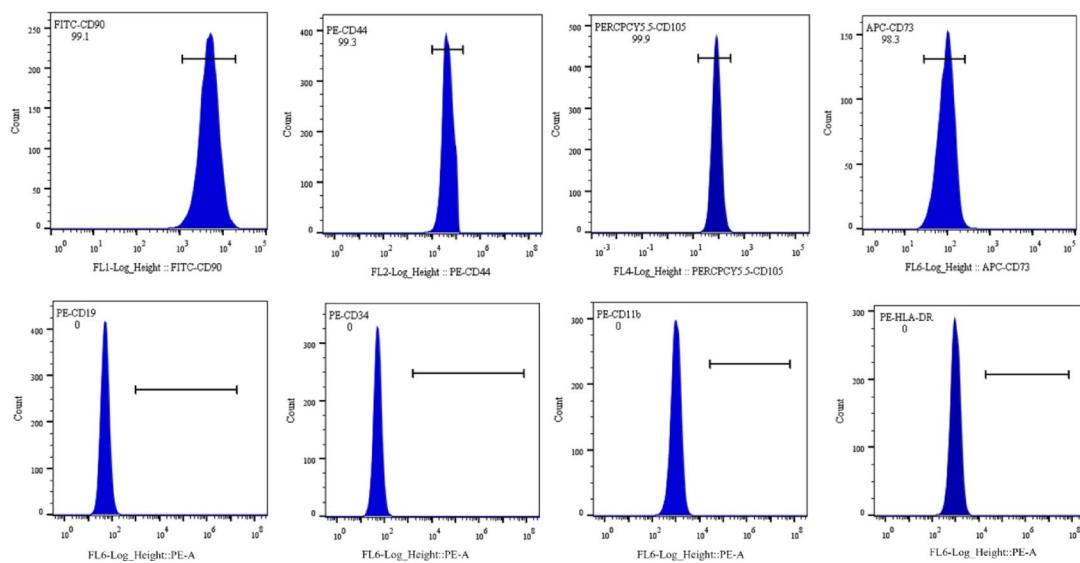


Fig. 1. Flow Cytometry Analysis Results of UC-MSCs.

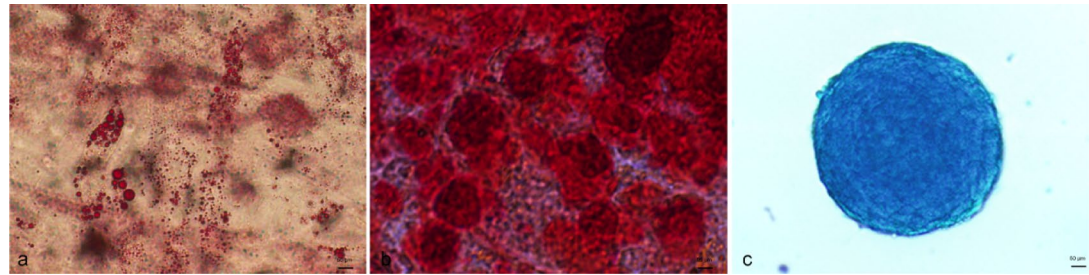


Fig. 2. Induction of UC-MSCs into Different Tissue Types. UC-MSCs induced into adipose tissue show red staining after Oil Red O staining (a). UC-MSCs induced into osteogenic tissue display red staining after Alizarin Red staining (b). UC-MSCs induced into chondrogenic tissue exhibit blue staining after Alcian Blue staining (c). All images are captured at a magnification of $\times 400$. Scale bar: 50 μ m.

Clinical pathological characteristics of UC-MSCs in improving thin endometrial morphology

The experimental animals were randomly divided into three groups: normal group, model group, and UC-MSCs group.

In the normal group, the average endometrial thickness of experimental rats, as assessed by H&E staining, was 0.44 ± 0.04 mm, with a clear endometrial structure, tightly arranged epithelial cells, and intact glandular structures with uniform numbers. The model group exhibited an average endometrial thickness of 0.11 ± 0.03 mm, indicating significant thinning of the endometrium, with loosely arranged epithelial cells, interrupted continuity, sparse glands, and disordered structures. In the UC-MSCs group, the average endometrial thickness was 0.34 ± 0.06 mm, which, while lower than that of the normal group, was significantly thicker than that of the model group ($p < 0.05$). The continuity of epithelial cells was relatively good, and while the glands were sparser than in the normal group, their number was significantly higher than that in the model group, and the structure was more intact (Fig. 3).

Endometrial fibrosis is an indicator of the degree of endometrial damage. The results of Masson staining showed that the fibrosis area in the model group accounted for approximately 28.14% (26.85%–30.62%) of the total endometrial area. In contrast, this proportion was about 11.22% (10.33%–12.39%) in the normal group and approximately 15.11% (13.82%–17.67%) in the UC-MSCs group. There was a significant difference between the model group and the UC-MSCs group ($p < 0.05$), indicating that UC-MSCs can repair the endometrium and inhibit the fibrosis of stromal connective tissue (Fig. 4).

Immunohistochemical staining for cytokeratin (CK) in tissue sections indicates the expression of keratin, with positive CK expression appearing as brown-yellow granules in the cytoplasm of epithelial cells. In the normal group, the average optical density of CK expression was 0.50 ± 0.07 , with uniformly distributed brown-yellow granules visible in the endometrial epithelial cells. The model group showed a CK average optical density of 0.27 ± 0.08 , with significantly fewer positive staining epithelial cells compared to the normal group. In contrast, the UC-MSCs group exhibited an average optical density of CK expression at 0.39 ± 0.09 , indicating

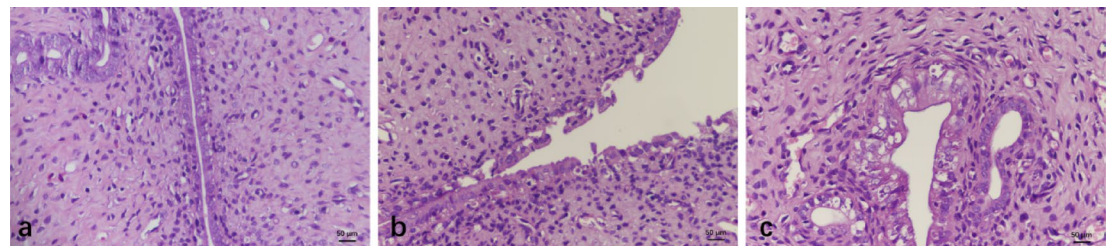


Fig. 3. H&E Staining of Endometrial Samples. Endometrium of the normal group (a). Endometrium of the model group (b). Endometrium of the UC-MSCs group (c). All images are captured at a magnification of $\times 400$. Scale bar: 50 μm .

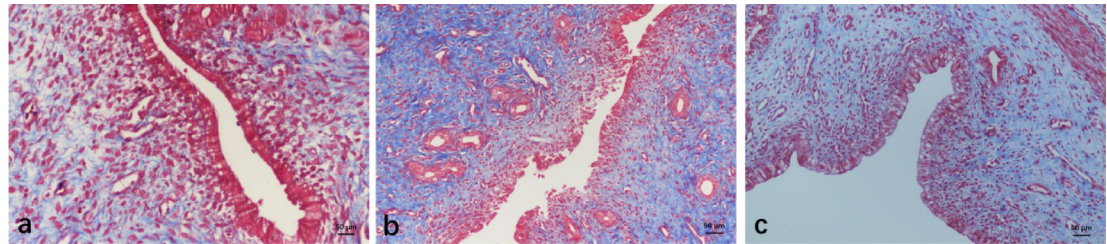


Fig. 4. Masson Staining of Endometrial Samples. Endometrium of the normal group (a), model group (b) and the UC-MSCs group (c). All images are captured at a magnification of $\times 400$. Scale bar: 50 μm .

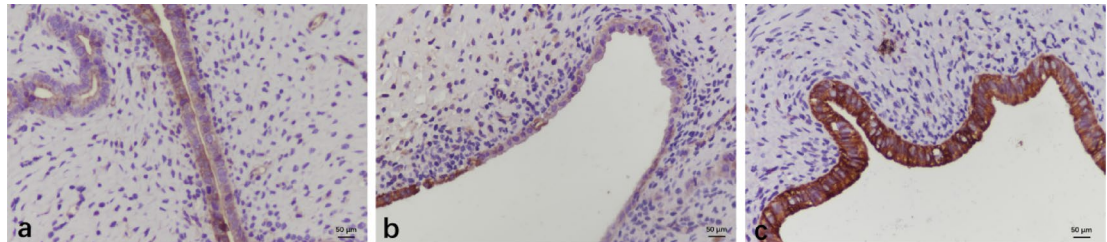


Fig. 5. CK Staining of Endometrial Samples. Endometrium of the normal group (a), model group (b) and the UC-MSCs group (c). All images are captured at a magnification of $\times 400$. Scale bar: 50 μm .

a significantly higher positive staining in endometrial epithelial cells compared to the model group ($p < 0.05$) (Fig. 5).

Ultrasound characteristics of UC-MSCs in improving thin endometrial morphology

Ultrasound imaging allows for dynamic observation of the endometrial thickness, morphology, continuity, and the presence of pregnancy within the uterine cavity (Fig. 6). In the normal group, the endometrial thickness and echogenicity were uniform, with the uterine cavity line visible and no obvious interruptions in continuity (Fig. 7a). In the model group, the endometrial thickness was significantly reduced and uneven, with multiple interruptions in the continuity of the uterine cavity line (Fig. 7b). The ultrasound images post-modeling corresponded with the anatomical and clinical pathological findings observed in the H&E stained images (Fig. 8). In the UC-MSCs group, the endometrial thickness showed a significant increase compared to post-modeling, with some visible repair of the interrupted uterine cavity line (Fig. 7).

Correlation and difference analysis between ultrasound measurements and clinical pathological measurements

Comparison of differences in endometrial thickness, number of glands in H&E staining, fibrosis area ratio in Masson staining, and average optical density of CK staining among normal, model, and UC-MSCs Groups (Table 1)

First, normality tests were performed to analyze the measurement data, specifically the H&E stained endometrial thickness, number of glands in H&E staining, and average optical density of CK staining, which were found to follow a normal distribution, denoted as $\bar{x} \pm s$. One-way ANOVA was then used for analysis, with pairwise comparisons conducted using the LSD-t test. In contrast, the Masson stained fibrosis area ratio data did not follow a normal distribution and were represented as M (Q1, Q3); the Mann-Whitney U test was employed

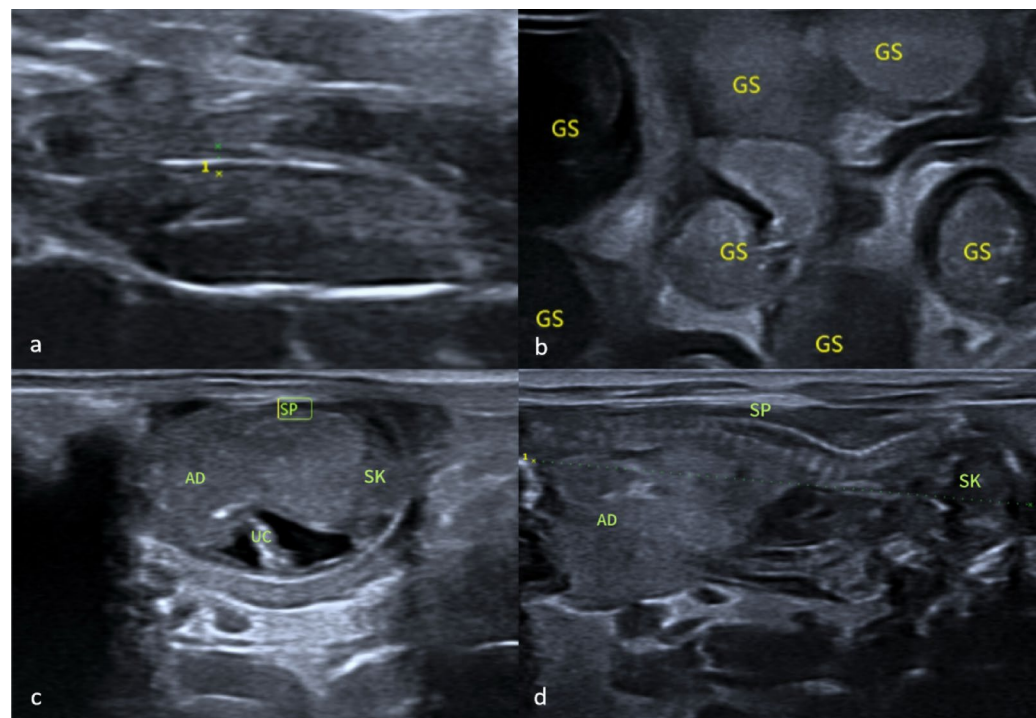


Fig. 6. Transabdominal ultrasound with the sagittal images demonstrating. Ultrasound image of the normal endometrium in a 14-week-old rat prior to pregnancy (a) and ultrasound images of the same rat during early, mid, and late stages of pregnancy, respectively (b, c, d). Annotations: GS (Gestational sac), SK (Skull), SP (Spine), AD (Abdomen), UC (Umbilical Cord).

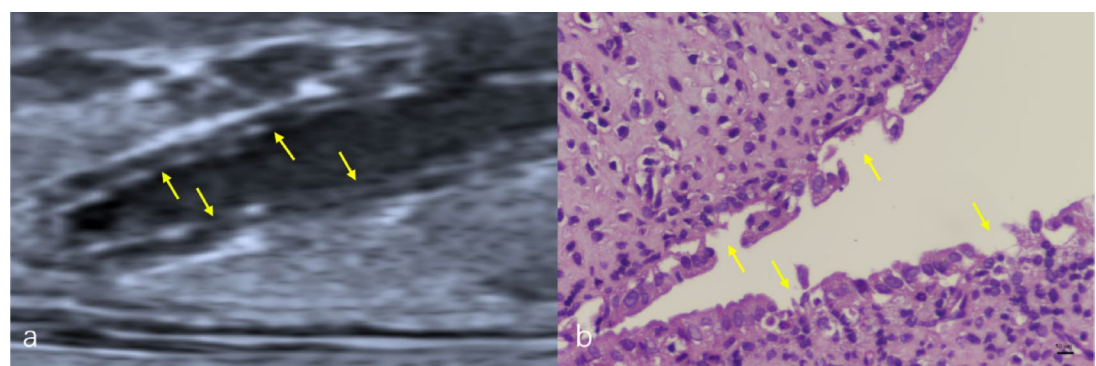


Fig. 7. Transabdominal ultrasound with the sagittal images demonstrating. Ultrasound image of the endometrium after modeling in the same rat (a) and clinical pathological H&E staining image following dissection (b). The pathological image is captured at a magnification of $\times 400$. Scale bar: 50 μm .

for analysis, with pairwise comparisons performed using Dunn's t test. A p-value of <0.05 was considered statistically significant.

The error bar graph in Fig. 9 illustrates the differences in H&E stained endometrial thickness, number of glands in H&E staining, Masson stained fibrosis area ratio, and average optical density of CK staining among the normal, model, and UC-MSCs groups in this study. The analysis revealed significant differences across the samples from the different groups for H&E stained endometrial thickness (mm), number of glands in H&E staining, Masson stained fibrosis area ratio, and average optical density of CK staining. Compared to the model group, both the normal group and the UC-MSCs group showed a significant increase in H&E stained endometrial thickness ($F=147.233, P<0.001$), as well as a significant increase in the number of glands in H&E staining ($F=147.305, P<0.001$).

The error bar graph in Fig. 10 shows that, compared to the model group, there was a significant reduction in Masson stained fibrosis after treatment with UC-MSCs ($F=89.333, P<0.0001$).

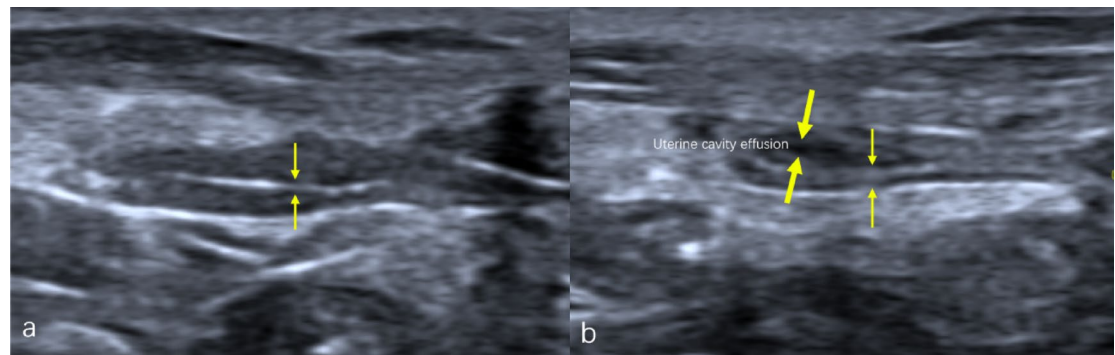


Fig. 8. Transabdominal ultrasound with the sagittal images demonstrating. Ultrasound image of the endometrium after modeling in the same rat (a) and ultrasound image of the endometrium after treatment with UC-MSCs (b). Endometrium (thin arrow), Uterine cavity effusion (thick arrow).

Group	<i>n</i>	H&E Stained Endometrial Thickness (mm)	Number of Glands in H&E Staining (count)	Masson Stained Fibrosis Area Ratio (%)	Average Optical Density of CK Staining
Normal	10	0.44 ± 0.04	31.08 ± 1.27	11.22 (10.33–12.39)	0.50 ± 0.07
Model	10	0.11 ± 0.03	16.13 ± 2.77	28.14 (26.85–30.62)	0.27 ± 0.08
UC-MSCs	10	0.34 ± 0.06	27.52 ± 1.76	15.11 (13.82–17.67)	0.39 ± 0.09

Table 1. Clinical characteristics of Groups.

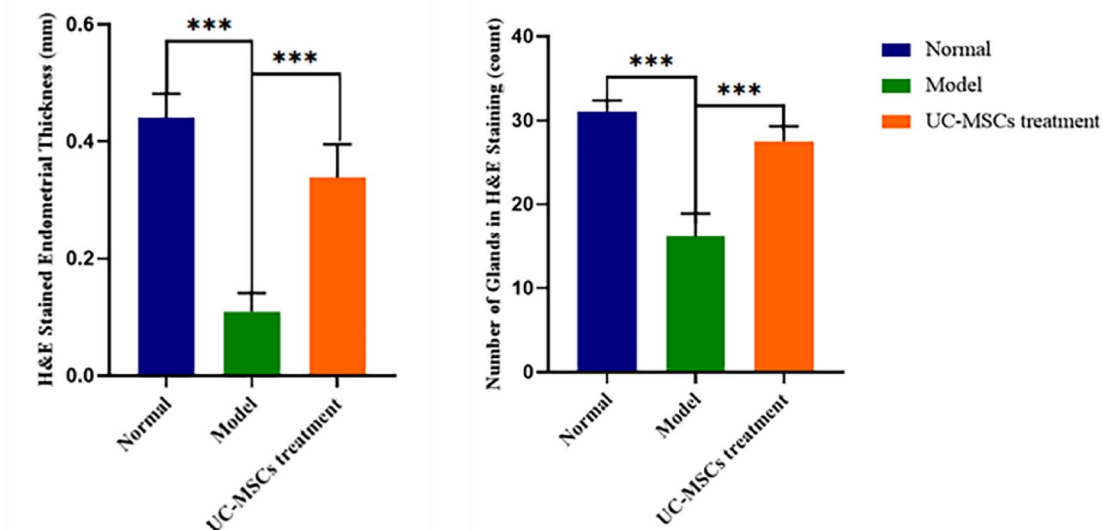


Fig. 9. The Promoting Effect of UC-MSCs Treatment on H&E Stained Glands. *** $P < 0.001$; ** $P < 0.01$; compared to the model group; $n = 10$.

The error bar graph in Fig. 11 demonstrates that, compared to the model group, both the normal group and the UC-MSCs group exhibited a significant increase in the average optical density of CK staining ($F = 21.334$, $P < 0.001$).

Correlation analysis between ultrasound measurements and clinical pathological measurements of H&E stained endometrial thickness

Using the data from the normal, model, and UC-MSCs groups for H&E stained endometrial thickness, correlation analysis was performed with the ultrasound measurements by parallelly assessing 10 samples of

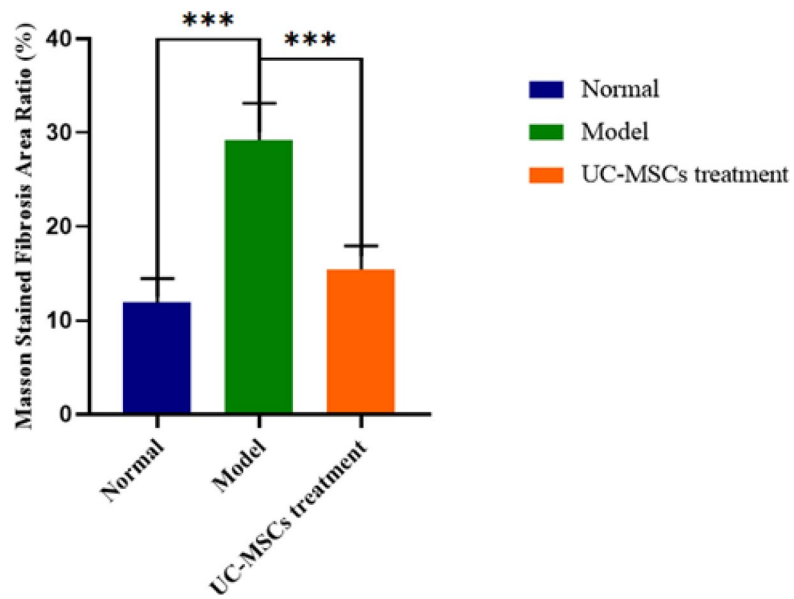


Fig. 10. The Inhibitory Effect of UC-MSCs Treatment on Masson Stained Fibrosis. *** $P < 0.001$; ** $P < 0.01$; compared to the model group; $n = 10$.

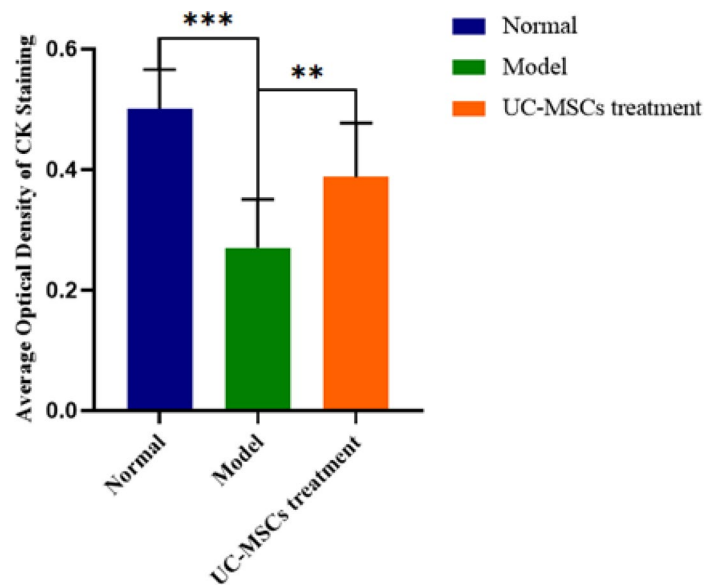


Fig. 11. The Promoting Effect of UC-MSCs Treatment on Average Optical Density of CK Staining. *** $P < 0.001$; ** $P < 0.01$; compared to the model group; $n = 10$.

H&E stained endometrial thickness data. The results, analyzed through linear regression, indicated that there were no significant differences between the two measurement methods ($r = 0.9991, 0.9992, 0.9995$ respectively; all $P < 0.0001$), demonstrating a strong correlation. The results are presented in Fig. 12.

Difference analysis between ultrasound measurements and clinical pathological measurements of H&E stained endometrial thickness

The comparison of ultrasound measurements and original measurements of H&E stained endometrial thickness among the normal group, model group, and UC-MSCs group showed no statistically significant differences ($P = 0.604, 0.823, 0.452$ respectively; all $P > 0.05$). The results are presented in Fig. 13.

Discussion

Normal embryos and good endometrial receptivity are essential factors for successful pregnancy¹⁷. Main causes of thin endometrium (less than 7 mm) include induced abortion, intrauterine surgery, and dysfunction of

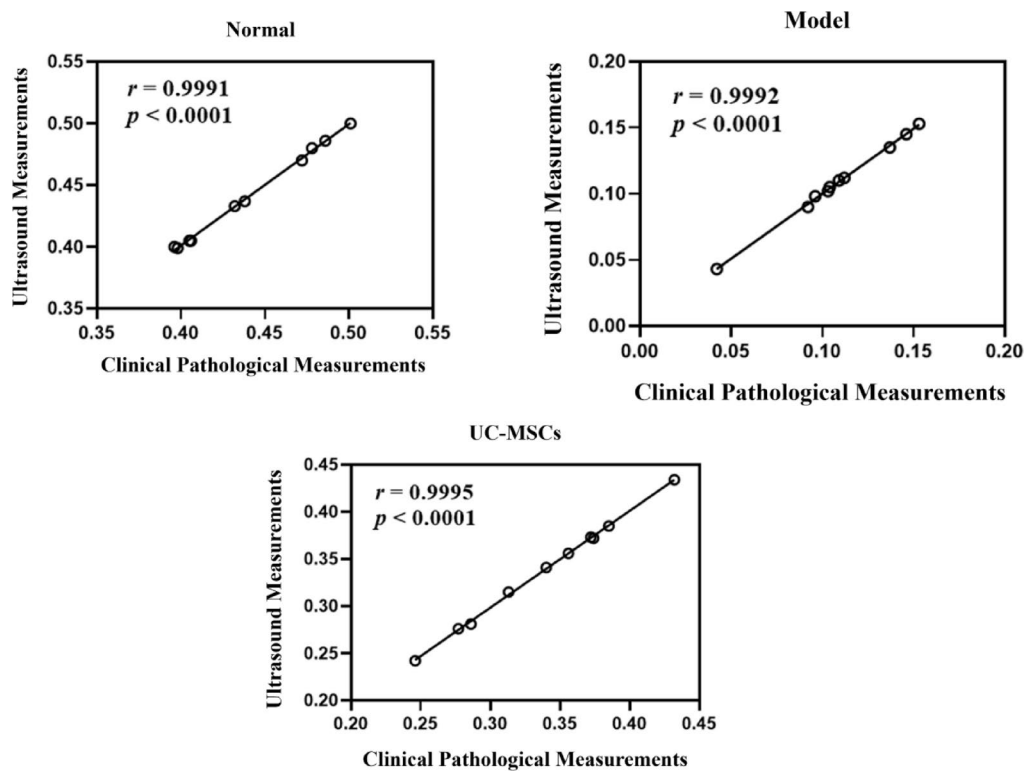


Fig. 12. Correlation Analysis between Ultrasound Measurements and Clinical Pathological Measurements of H&E Stained Endometrial Thickness.

endometrial stem/progenitor cells¹⁸. It has been reported that thin endometrium is associated with lower embryo implantation rates^{5,6,19,20} and is linked to a higher incidence of early miscarriage (including spontaneous abortion and ectopic pregnancy), intrauterine growth restriction, and adverse perinatal outcomes^{21,22}. Additionally, patients with thin endometrium have a twofold increased risk of low birth weight and preterm birth²³.

Ultrasound is a safe and non-invasive examination method that can visually, dynamically, and comprehensively display the observed area. In this study, we explore for the first time the application value of ultrasound imaging in an animal experiment involving stem cell therapy for intrauterine adhesions. This method allows for a comprehensive observation of the conditions within the uterine cavity in a living organism. In contrast, clinical pathological studies conducted post-dissection may exhibit significant randomness in results due to limitations in sample collection and other factors. In our study, we assessed changes in endometrial receptivity in rats before and after treatment by measuring endometrial thickness and observing the morphology and continuity of the endometrium. The data obtained were compared for correlation and differences with the results from ex vivo studies, revealing no statistically significant differences between in vivo and ex vivo values. In summary, our research demonstrates that UC-MSCs can repair the impaired endometrial receptivity in rats, which can be indicated through ultrasound imaging in a living state, providing a theoretical foundation for future research in this field.

Conclusion

This study establishes ultrasound as a non-invasive tool for real-time in vivo monitoring of UC-MSCs efficacy in restoring endometrial receptivity in IUA, overcoming limitations of terminal histology. In this study, we found that UC-MSCs can promote the recovery of the structure and function of the damaged endometrium. Ultrasound, as a non-invasive examination method, allows for real-time monitoring of endometrial thickness, morphology, and continuity of the uterine cavity line, thereby indicating the progress of animal experiments through in vivo studies. This approach is more convenient and quicker compared to ex vivo studies and enables effective preoperative assessment of endometrial regeneration. In comparison to the ultrasonic skin imager (model DUB, 50 MHz, TMP, Germany), the small animal ultrasound device used in this study (Vinson, VINNO6LAB, 18 MHz, Suzhou, China) has lower image clarity and resolution. However, with future advancements in small animal ultrasound imaging, including significant improvements in image clarity and resolution, as well as further optimization of functionality, it is anticipated that three-dimensional energy Doppler ultrasound and VOCAL software will enable automatic calculations of endometrial volume, vascularization index, blood flow index, and vascularization-blood flow index. This will provide a more precise evaluation of endometrial angiogenesis and receptivity. We believe that our ultrasound research offers a new avenue for clinical animal experiments.

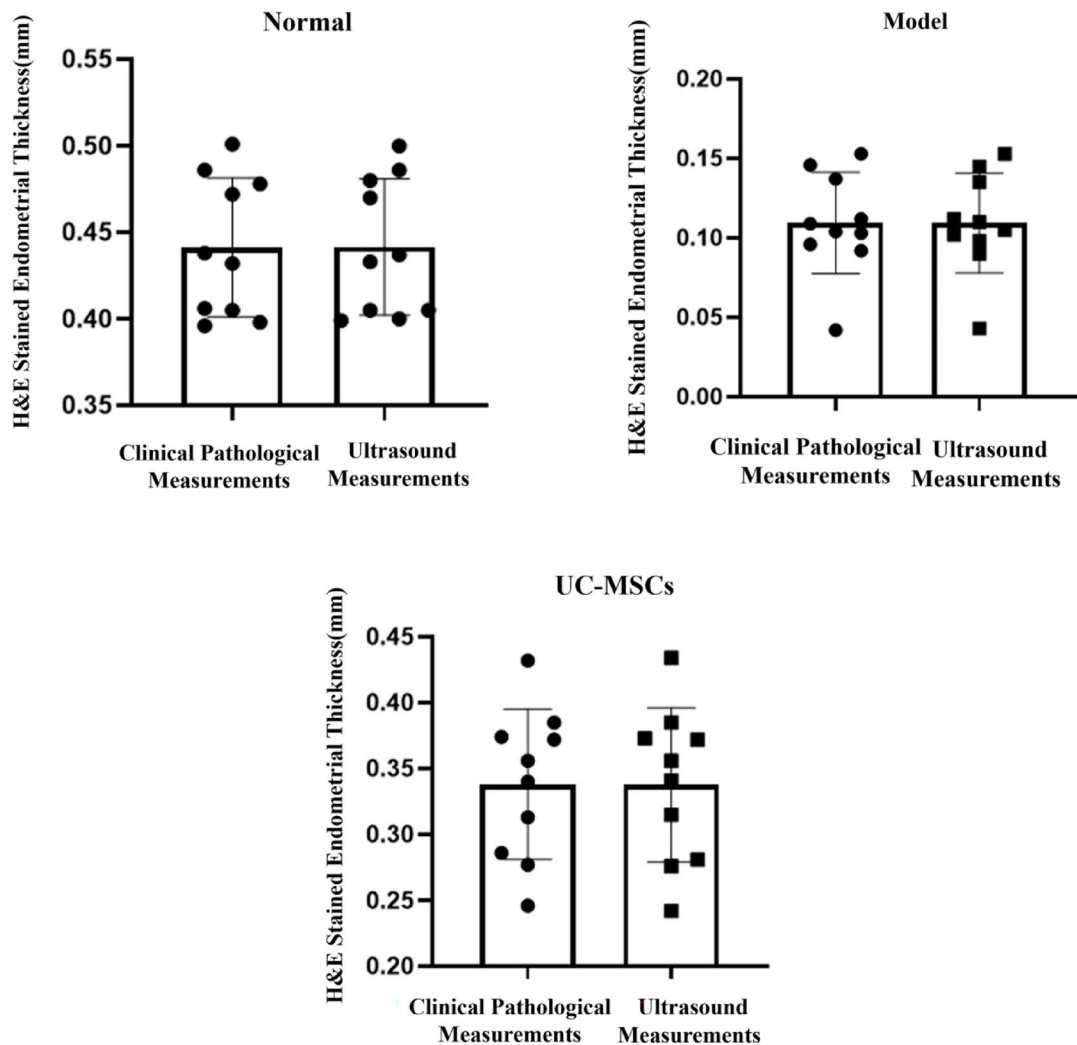


Fig. 13. Difference Analysis between Ultrasound Measurements and Clinical Pathological Measurements of H&E Stained Endometrial Thickness.

Data availability

The UC-MSCs data generated by this study have been deposited in the Science Date Bank database (DOI: <https://doi.org/10.57760/sciencedb.19158>). Other datasets used and analysed during the current study are available from the corresponding author on reasonable request.

Received: 17 March 2025; Accepted: 5 August 2025

Published online: 11 August 2025

References

1. Dreisler, E. & Kjer, J. J. Asherman's syndrome: current perspectives on diagnosis and management. *Int. J. Womens Health.* **11**, 191–198. <https://doi.org/10.2147/IJWH.S165474> (2019). Published 2019 Mar 20.
2. Senturk, L. M. & Erel, C. T. Thin endometrium in assisted reproductive technology. *Curr. Opin. Obstet. Gynecol.* **20** (3), 221–228. <https://doi.org/10.1097/GCO.0b013e328302143c> (2008).
3. Liu, K. E., Hartman, M. & Hartman, A. Management of thin endometrium in assisted reproduction: a clinical practice guideline from the Canadian fertility and andrology society. *Reprod. Biomed. Online.* **39** (1), 49–62. <https://doi.org/10.1016/j.rbmo.2019.02.013> (2019).
4. Moustafa, S. M., Garneau, A. S. & Goodman, L. R. Elusive effect of endometrial Thickness: through Thick and thin. *Fertil. Steril.* **115** (1), 89–90. <https://doi.org/10.1016/j.fertnstert.2020.09.135> (2021).
5. Sarvi, F., Arabahmadi, M., Alleyassin, A., Aghahosseini, M. & Ghasemi, M. Effect of increased endometrial thickness and implantation rate by granulocyte Colony-Stimulating factor on unresponsive thin endometrium in fresh in vitro fertilization cycles: A randomized clinical trial. *Obstet. Gynecol. Int.* **2017**, 3596079. <https://doi.org/10.1155/2017/3596079> (2017).
6. von Wolff, M. et al. Thin endometrium is also associated with lower clinical pregnancy rate in unstimulated menstrual cycles: A study based on natural cycle IVF. *Front. Endocrinol. (Lausanne).* **9**, 776. <https://doi.org/10.3389/fendo.2018.00776> (2018). Published 2018 Dec 20.
7. Sebag, L. et al. Early Second-Look hysteroscopy: prevention and treatment of intrauterine Post-surgical adhesions. *Front. Surg.* **6**, 50. <https://doi.org/10.3389/fsurg.2019.00050> (2019). Published 2019 Aug 16.

8. Khan, Z. & Etiology Risk factors, and management of Asherman syndrome. *Obstet. Gynecol.* **142** (3), 543–554. <https://doi.org/10.1097/AOG.0000000000005309> (2023).
9. Zhang, L. et al. Transplantation of umbilical cord-derived mesenchymal stem cells promotes the recovery of thin endometrium in rats. *Sci Rep.* ;12(1):412. Published 2022 Jan 10. (2022). <https://doi.org/10.1038/s41598-021-04454-7>
10. Hua, Q. et al. Human umbilical cord blood-derived MSCs trans-differentiate into endometrial cells and regulate Th17/Treg balance through NF- κ B signaling in rabbit intrauterine adhesions endometrium. *Stem Cell Res Ther.* ;13(1):301. Published 2022 Jul 15. (2022). <https://doi.org/10.1186/s13287-022-02990-1>
11. Wang, Y., Tang, Z. & Teng, X. New advances in the treatment of thin endometrium. *Front. Endocrinol. (Lausanne)*. **15**, 1269382. <https://doi.org/10.3389/fendo.2024.1269382> (2024). Published 2024 Apr 30.
12. Sun, X. C. et al. Combining bone collagen matrix with HUC-MSCs for application to alveolar process cleft in a rabbit model. *Stem Cell. Rev. Rep.* **19** (1), 133–154. <https://doi.org/10.1007/s12015-021-10221-y> (2023).
13. Hoang, D. M. et al. Stem cell-based therapy for human diseases. *Signal. Transduct. Target. Ther.* **7** (1), 272. <https://doi.org/10.1038/s41392-022-01134-4> (2022). Published 2022 Aug 6.
14. Santamaria, X., Mas, A., Cervelló, I., Taylor, H. & Simon, C. Uterine stem cells: from basic research to advanced cell therapies. *Hum. Reprod. Update.* **24** (6), 673–693. <https://doi.org/10.1093/humupd/dmy028> (2018).
15. Zhang, L. et al. Therapeutic effect of human umbilical cord-derived mesenchymal stem cells on injured rat endometrium during its chronic phase. *Stem Cell Res Ther.* ;9(1):36. Published 2018 Feb 13. (2018). <https://doi.org/10.1186/s13287-018-0777-5>
16. Pu, X. et al. Human UC-MSC-derived exosomes facilitate ovarian renovation in rats with chemotherapy-induced premature ovarian insufficiency. *Front Endocrinol (Lausanne)*. ;14:1205901. Published 2023 Jul 26. (2023). <https://doi.org/10.3389/fendo.2023.1205901>
17. Vartanyan, E., Tsaturova, K. & Devyatova, E. Thin endometrium problem in IVF programs. *Gynecol. Endocrinol.* **36** (sup1), 24–27. <https://doi.org/10.1080/09513590.2020.1816724> (2020).
18. Caserta, M. P., Bolan, C. & Clingan, M. J. Through Thick and thin: a pictorial review of the endometrium. *Abdom. Radiol. (NY)*. **41** (12), 2312–2329. <https://doi.org/10.1007/s00261-016-0930-5> (2016).
19. Ziganshina, M. M. et al. Epithelial apical glycosylation changes associated with thin endometrium in women with infertility - a pilot observational study. *Reprod Biol Endocrinol.* ;19(1):73. Published 2021 May 15. (2021). <https://doi.org/10.1186/s12958-021-00750-z>
20. Jacobs, E. A. et al. Endometrial thickness: how thin is too thin? *Fertil. Steril.* **118** (2), 249–259. <https://doi.org/10.1016/j.fertnstert.2022.05.033> (2022).
21. Zheng, Y. et al. Thin endometrium is associated with higher risks of preterm birth and low birth weight after frozen single blastocyst transfer. *Front Endocrinol (Lausanne)*. ;13:1040140. Published 2022 Nov 10. (2022). <https://doi.org/10.3389/fendo.2022.1040140>
22. Oron, G. et al. Endometrial thickness of less than 7.5 mm is associated with obstetric complications in fresh IVF cycles: a retrospective cohort study. *Reprod. Biomed. Online.* **37** (3), 341–348. <https://doi.org/10.1016/j.rbmo.2018.05.013> (2018).
23. Mouhayer, Y., Fransaliak, J. M. & Sharara, F. I. Obstetrical complications of thin endometrium in assisted reproductive technologies: a systematic review. *J. Assist. Reprod. Genet.* **36** (4), 607–611. <https://doi.org/10.1007/s10815-019-01407-y> (2019).

Acknowledgements

We grateful acknowledge project supported by Shandong Provincial Natural Science Foundation (Grant No. ZR2021MH046); the Central Laboratory of Yantai Yuhuangding Hospital of Qingdao University for providing a well-equipped platform. The authors declare that they have not use AI-generated work in this manuscript" in this section.

Author contributions

Guarantors of integrity of entire study M.L., S.G.; study concepts/study design M.L., S.G.; data acquisition or data analysis/interpretation, all authors; manuscript drafting or manuscript revision for important intellectual content all authors; approval of final version of submitted manuscript, all authors; agrees to ensure any questions related to the work are appropriately resolved, all authors.

Funding information

Shandong Provincial Natural Science Foundation (Grant No. ZR2021MH046).

Declarations

Consent for publication

Not applicable.

Competing interests

The authors declare no competing interests.

Ethics declarations

UC-MSCs and all animals studies have been approved by Ethics Committee of Yantai Yuhuangding Hospital (NO.2024-554), Date of approval: 2024.07.05 . And the title of the approved project is " Mechanism Study on Continuous 3D-PDA Ultrasound Evaluation of Umbilical Cord Mesenchymal Stem Cells and Their Exosomes in Treating Thin Endometrium and Improving Embryo Transfer Outcome". All animal experiments conform to the Animal Research: Reporting of In Vivo Experiments (ARRIVE) guidelines. This study did not involve human subjects.

Additional information

Correspondence and requests for materials should be addressed to M.L.

Reprints and permissions information is available at www.nature.com/reprints.

Publisher's note Springer Nature remains neutral with regard to jurisdictional claims in published maps and institutional affiliations.

Open Access This article is licensed under a Creative Commons Attribution-NonCommercial-NoDerivatives 4.0 International License, which permits any non-commercial use, sharing, distribution and reproduction in any medium or format, as long as you give appropriate credit to the original author(s) and the source, provide a link to the Creative Commons licence, and indicate if you modified the licensed material. You do not have permission under this licence to share adapted material derived from this article or parts of it. The images or other third party material in this article are included in the article's Creative Commons licence, unless indicated otherwise in a credit line to the material. If material is not included in the article's Creative Commons licence and your intended use is not permitted by statutory regulation or exceeds the permitted use, you will need to obtain permission directly from the copyright holder. To view a copy of this licence, visit <http://creativecommons.org/licenses/by-nc-nd/4.0/>.

© The Author(s) 2025